1-1-2015

Stochastic Interdigitation As a Toughening Mechanism at the Interface between Tendon and Bone

Y. Hu

Victor Birman
Missouri University of Science and Technology, vbirman@mst.edu

A. Demyier-Black

A. G. Schwartz

et. al. For a complete list of authors, see http://scholarsmine.mst.edu/mec_aereng_facwork/3742

Recommended Citation

Y. Hu et al., "Stochastic Interdigitation As a Toughening Mechanism at the Interface between Tendon and Bone," *Biophysical Journal*, vol. 108, no. 2, pp. 431-437, Biophysical Society, Jan 2015.
The definitive version is available at https://doi.org/10.1016/j.bpj.2014.09.049

Article

Stochastic Interdigitation as a Toughening Mechanism at the Interface between Tendon and Bone

Yizhong Hu,[1,2] Victor Birman,[3] Alix Demyier-Black,[4] Andrea G. Schwartz,[4] Stavros Thomopoulos,[1,2,4,*] and Guy M. Genin[2,*]

[1]Department of Biomedical Engineering and [2]Department of Mechanical Engineering and Materials Science, Washington University, St. Louis, Missouri; [3]Engineering Education Center, Missouri Science & Technology, St. Louis, Missouri; and [4]Department of Orthopaedic Surgery, Washington University School of Medicine, St. Louis, Missouri

ABSTRACT Reattachment and healing of tendon to bone poses a persistent clinical challenge and often results in poor outcomes, in part because the mechanisms that imbue the uninjured tendon-to-bone attachment with toughness are not known. One feature of typical tendon-to-bone surgical repairs is direct attachment of tendon to smooth bone. The native tendon-to-bone attachment, however, presents a rough mineralized interface that might serve an important role in stress transfer between tendon and bone. In this study, we examined the effects of interfacial roughness and interdigital stochasticity on the strength and toughness of a bimaterial interface. Closed form linear approximations of the amplification of stresses at the rough interface were derived and applied in a two-dimensional unit-cell model. Results demonstrated that roughness may serve to increase the toughness of the tendon-to-bone insertion site at the expense of its strength. Results further suggested that the natural tendon-to-bone attachment presents roughness for which the gain in toughness outweighs the loss in strength. More generally, our results suggest a pathway for stochasticity to improve surgical reattachment strategies and structural engineering attachments.

INTRODUCTION

The tendon-to-bone insertion presents a structured, hierarchical, and orderly arrangement of proteins and mineral to achieve effective attachment between two very different tissues (1,2). Many levels of this hierarchical tissue system do not regenerate after injury (3–5). For example, after surgical repair of rotator cuff injuries, the rate of recurrence of tears ranges from 20% in the best-case scenario to as high as 94% in some patient populations (6). The strength and toughness of the healthy tendon-to-bone insertion is known to rely on a combination of structural and compositional features across scales, including the following:

1. Mineral-protein interactions at the nanoscale (7,8),
2. Gradients in mineral content and collagen fiber organization at the microscale (9,10), and
3. Functional grading at the millimeter scale (1,11,12).

Our long-term goal is to reduce failure rates after tendon-to-bone reattachment surgeries by identifying strengthening and toughening mechanisms in the healthy tendon-to-bone insertion and by developing strategies for reconstituting these surgically.

Our focus here is something of an anomaly in the orderly hierarchical structure of the tissue that bridges tendon and bone: a wavy, irregular interface that results in interdigitation between the two tissues. For example, at the rotator cuff in the shoulder, the supraspinatus tendon forms an interdigitating interface with the humeral head with stochastic finger lengths (Fig. 1). We hypothesize that this stochasticity is a toughening mechanism that enables the tendon-to-bone interface to absorb more strain energy before failure. Such toughening mechanisms are crucial for mechanically competent materials and interfaces, but often present a dilemma: procedures that toughen a material characteristically reduce its strength. Examples of this trade-off include annealing in metals (13) and introduction of compliant interfaces in fibrous laminate composites (14–18). The classic Coleman (19) solution for fibrous materials shows that that rope bundle strength reduces proportional to the variance of the mechanics of the fibers that comprise it. However, in fibrous composites, analogous stochasticity in fiber strength can increase toughness (20,21). Biological tissues are typically much more regular than rope or engineering composites, but we hypothesized that stochastic interdigitation finger lengths would reduce attachment strength in exchange for higher toughness.

Interdigitations are present throughout nature at interfaces such as those found in nacre (22,23), armored fish (24), algae (25), and sutures within the skull (26) and jaw (27). Interdigitations are believed to improve load transmission and increase energy absorption of the interfaces between bones in the skull (28). Advanced micromechanical models exist for a range of these interfaces (29,30). However, all of these interfaces differ fundamentally from the attachment of tendon to bone in that they feature a relatively

Submitted May 12, 2014, and accepted for publication September 30, 2014.

*Correspondence: genin@wustl.edu or thomopouloss@wustl.edu

Editor: Nathan Baker.

0006-3495/15/01/0431/7 $2.00

http://dx.doi.org/10.1016/j.bpj.2014.09.049

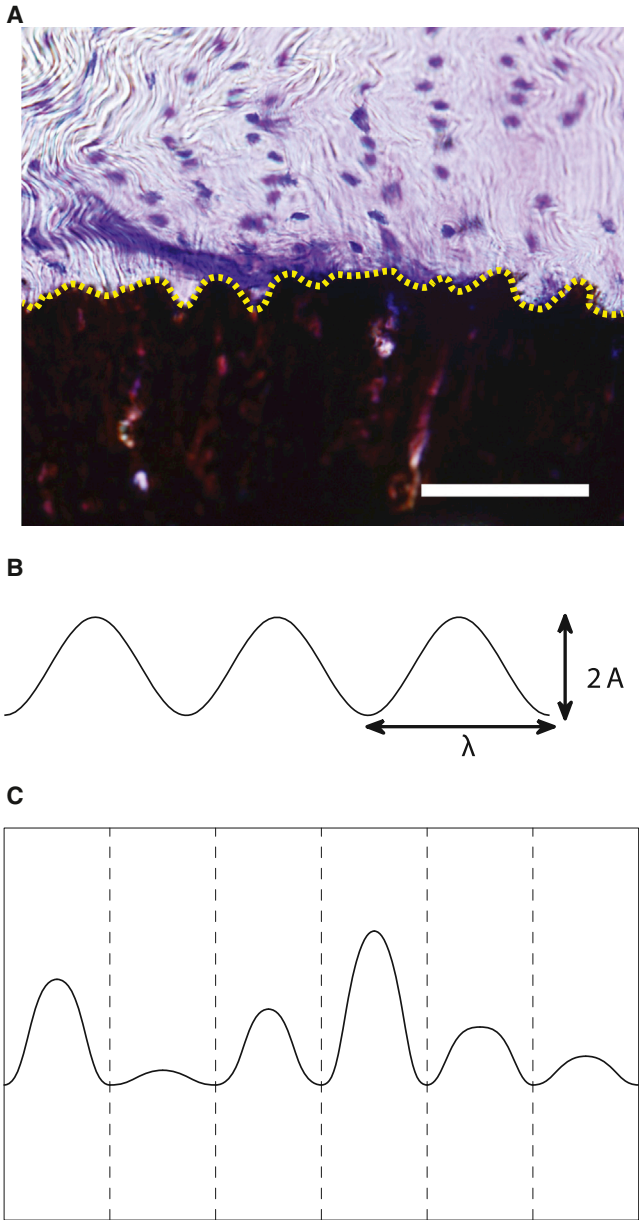

FIGURE 1 (*A*) Image of the tendon-to-bone attachment site at a mouse rotator cuff, stained with von Kossa (*black*) and toluidine blue. The mineralized tissue is stained black and the unmineralized tissue is stained purple. (*Dotted yellow line*) Interdigitation at the interface, which roughly resembles a sinusoidal wave with approximately the same width but varying amplitude. (Scale bar: 50 μm). (*B*) Definition of variables in the perturbation model. A sinusoid with wavelength λ and amplitude A was used to model the interface. (*C*) The Monte Carlo simulation was constructed by combining multiple strips of constant width. Each strip had a tendon region (*top*) and a bone region (*bottom*), separated by a single period of a cosine wave. The value for the amplitude was chosen from a normal distribution with assigned mean and standard deviation. (*Arrows*) Applied tensile displacement perpendicular to the boundary between tendon and bone. To see this figure in color, go online.

compliant seam between two relatively stiff materials. In contrast, the attachment of tendon to bone involves direct attachment of a highly compliant material (tendon) to a stiff one (bone). A key feature of the analyses in this study is therefore the analysis of stress concentrations. Whereas these can be ignored reasonably at a compliant seam between interdigitating bone plates, they are a central feature of the mechanics of the tendon-to-bone interface. These stress concentrations become more severe with increasing sharpness of the interdigitating features and, we argue, underlie a trade-off between toughening and weakening that must be optimized at these interfaces.

In this work, we quantified the effects of a rough and randomized boundary on the mechanical properties of a bimaterial interface through an analytical approximation of the stress field. A first-order model is applied to capture the scalings of how interdigitation can affect strength and toughness at an interface between dissimilar materials. Our results suggested a range of interfacial morphologies that could serve to enhance toughness.

MATERIALS AND METHODS

Our modeling efforts were motivated by observations that the supraspinatus tendon-to-bone insertion in mice presents highly stochastic interdigitation between tendon and bone. The methods used to acquire and interpret these images are described in the first section below. We developed a closed form perturbation solution to evaluate possible benefits, such as increased surface area and improved toughness, that might arise from such an interface, but found that interdigitation between two dissimilar materials always serves to amplify interfacial stresses. The derivation is summarized below, and presented in detail in the Supporting Material along with finite element analyses used to validate the solution. Finally, we considered the effect on toughness of the tendon-to-bone attachment site by combining up to 500 rectangular unit cells, each containing a tendon region and a bone region separated by a sinusoidal boundary. The unit cells were combined so that the sinusoidal interface formed a continuous boundary. Finally, we describe simulations and toughness measures used to show how interdigitation might enhance interfacial toughness.

Specimen preparation and image analysis

The specimens studied were mouse supraspinatus tendon attachments into humeral head bone ($N = 6$). All procedures for the handling of animals were approved by the Washington University Animal Studies Committee. The tendon-bone constructs were freshly dissected, immediately embedded in optimum cutting temperature medium, and frozen at -80°C. The embedded samples were cut into 30-μm-thick sections via a cryo-microtome, and the sections were deposited onto glass slides. The sections were then stained with von Kossa and toluidine blue stains to identify the mineral (*black*) and the proteoglycans/cells (*purple/blue*) via optical microscopy (Fig. 1 *A*). The boundary between the black region and purple region was identified as the tendon-bone interface.

Images of the attachment sites were analyzed by direct measurement. The tendon-bone interface was divided into segments, each containing a single protrusion of the bone into the tendon. The widths and heights of the protrusions were defined as λ and $2A$ (Fig. 1 *B*), respectively, and were measured using tools native to the IMAGEJ environment (31). The ratio of A/λ was recorded for each protrusion. Note that in the continuum frameworks applied here, stress and strain calculations are free of absolute scales (32). Therefore, the ratio between height and width, defined as the aspect ratio A/λ, was used in subsequent stress analysis as an indication of the degree of interdigitation throughout the study. The mean and standard deviation of the aspect ratio were also calculated. In the six

mice studied, >100 interdigitations between tendon and bone were sampled. At this sample size, our study yields a margin of error under 10% of the calculated mean at the 95% confidence level, and is thus likely representative for the mouse rotator cuff attachment.

Analytical procedures

We developed an approximate linear elasticity solution for the mechanical fields arising at the interface between two linear elastic, isotropic solids. The complete derivation is listed in the Supporting Material. The solution considered a wavy interface between two isotropic materials subject to tensile stress σ_∞. The shape of the interface was represented by a cosine wave,

$$\begin{aligned} y(x) &= A\cos kx, \\ k &= 2\pi/\lambda, \end{aligned} \tag{1}$$

where A and λ were the amplitude and wavelength of the cosine wave, respectively. The y axis was directed along the tendon-bone axis, and the x axis was directed perpendicular to this. The estimate was based upon a perturbation solution for an analogous problem, published by Gao (33). As described in the Supporting Material, the stress fields in the tendon and bone, denoted by subscripts 1 and 2, respectively, could be approximated as

$$\begin{aligned} (\sigma_{xx}(x,y))_1 &= 1/2Ake^{-ky}(\Omega(3-2ky)+\Pi)\sigma_\infty\cos kx, \\ (\sigma_{yy}(x,y))_1 &= (1+1/2Ake^{-ky}(\Omega(2ky+1)-\Pi)\cos kx)\sigma_\infty, \\ (\sigma_{xy}(x,y))_1 &= 1/2Ake^{-ky}(\Omega(2ky-1)-\Pi)\sigma_\infty\sin kx, \\ (\sigma_{xx}(x,y))_2 &= 1/2Ake^{ky}(\Pi(2ky-3)-\Omega)\sigma_\infty\cos kx, \\ (\sigma_{yy}(x,y))_2 &= (1-1/2Ake^{ky}(\Pi(2ky+1)-\Omega)\cos kx)\sigma_\infty, \\ (\sigma_{xy}(x,y))_2 &= 1/2Ake^{ky}(\Pi(2ky-1)-\Omega)\sigma_\infty\sin kx, \end{aligned} \tag{2}$$

The dimensionless parameters Ω and Π represent the mismatch in material properties between materials 1 and 2,

$$\Omega = \frac{1/\mu_1 - 1/\mu_2}{\kappa_1/\mu_1 + 1/\mu_2}, \tag{3}$$

$$\Pi = \frac{1/\mu_2 - 1/\mu_1}{\kappa_2/\mu_2 + 1/\mu_1}, \tag{4}$$

where μ_1 and μ_2 represent the shear moduli of materials 1 and 2, respectively, and, for the case of plane strain considered, $\kappa_1 = 3–4\nu_1$ and $\kappa_2 = 3–4\nu_2$, in which ν_1 and ν_2 are the Poisson ratios for materials 1 and 2, respectively. Analogous expressions exist for plane stress (see the Supporting Material). The linear elastic material properties used were $E_1 = 400$ MPa and $\nu_1 = 0.49$ for tendon, and $E_2 = 20$ GPa and $\nu_2 = 0.3$ for bone. Although neither tissue is a linear elastic or isotropic solid, these numbers are reasonable linear approximations and have been shown elsewhere to suffice for representing the role of the elastic mismatch in tendon-to-bone mechanics (34–38). Stress tensors were then constructed with the components estimated using the expressions in Eq. 2, and the maximum in-plane principal and shear stresses were identified.

Numerical procedures

Validation of perturbation solution

To verify the analytical solutions, we performed finite element analyses on unit cell models using a commercial finite element package (SIMULIA ABAQUS FEA; Dassault Systemès, Waltham, MA). As described in detail in the Supporting Material, each rectangular unit cell contained half of a bone/tendon sinusoidal finger (Fig. 1). A range of height (length in the tendon-to-bone axis direction) to width ratios was studied, with most simulations having a height/width ratio of 0.1. These domains were discretized with ~3500 triangular, quadratic interpolation elements (~10,000 degrees of freedom; see Fig. S3) to ensure convergence (see Fig. S5). Standard boundary conditions were used for the unit cell (e.g., Genin and Hutchinson (17)), with periodic boundary conditions on the lateral and bottom faces. The top face of each unit cell was displaced a prescribed amount in the tendon-bone axis direction, and kept shear-free. We first performed convergence studies by calculating both the total energy and the peak stresses as we increased the number of nodes and elements of the mesh. A mesh size for which the stress values converged was determined and maintained for the subsequent analysis.

A series of simulations were run to assess the range of validity of the model. In these simulations, the roughness amplitude A was increased while the unit cell length and width were kept constant. The error in peak in-plane principal stress was very small (<10%) for $A/\lambda < 0.2$, but increased rapidly for higher roughness amplitudes (see Fig. S7).

Simulations of strength and toughness

Using Monte Carlo methods, we represented the tendon-to-bone insertion site with up to 500 unit cells, each with the degree of interdigitation A/λ assigned according to a prescribed normal distribution. The width of the unit cells, λ, was kept constant at 1. The mean value and standard deviation of A/λ were varied to determine the effects of roughness and stochasticity on toughness and load-bearing ability of the interface. The height of each unit cell was set to 20 times the width.

A controlled displacement perpendicular to the interface was applied in a tensile manner to the composite model, similar to the loading mode of tendon in vivo (Fig. 1). Using the perturbation solution, the principal stress along the boundary between tendon and bone in each unit cell was calculated as the interface was stretched continuously. As a first-order model, strips were not considered to affect the stress fields of their neighbors, and a strip was considered to have failed when the peak stress along its interface exceeded the maximum allowable stress. Due to the nonuniform interdigitation, some strips failed at lower loads than others. When the maximum principal stress in a strip reached a prescribed critical value, it ceased to bear tensile load, and the load it bore was distributed among the rest of the intact unit cells. Finite element analyses of unit cells indicated that the effect of A on the stiffness of each unit cell was sufficiently small to be neglected, so the loads were distributed evenly among all intact unit cells. The simulation ended when all strips failed. A more detailed description of the simulation can be found in the Supporting Material.

The strength (peak load) and toughness (area under the force-displacement curve) of each composite model were estimated from the force displacement curves. Thirty simulations were performed for each value of mean A/λ to extract the dependence of strength and toughness on the mean and standard deviation of the amplitude distribution.

RESULTS

Stained images of tendon-to-bone insertion sites showed a sharp contrast between mineralized and nonmineralized regions (Fig. 1 *A*). Analysis of these images indicated that the degree of interdigitation (A/λ) followed an approximately normal distribution centered at 0.14, with a standard deviation of $s = 0.53$ (normalized by the mean) (Fig. 2).

Fixing the degree of interdigitation at $A/\lambda = 0.2$ and gradually introducing spread in the distribution (i.e., increasing the standard deviation, s), the Monte Carlo simulations suggested that as s decreased, the maximum load that a tendon-to-bone insertion site could sustain decreased, but

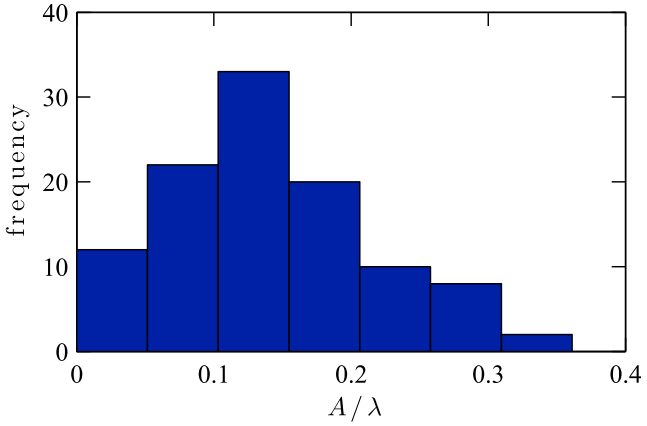

FIGURE 2 Physiological data from six mouse tendon-to-bone attachments show that the ratios of height and width of the protrusions followed an approximately normal distribution with a slight right skew. These values represent a sample size of >100 interdigitations in the six mice studied, yielding a margin of error <10% at the 95% confidence level. The mean value was 0.14 and the standard deviation was 0.53 when normalized by the mean. To see this figure in color, go online.

the displacement to ultimate failure of the composite model increased (Fig. 3). When the distribution was uniform ($s = 0$), every strip of the interface failed simultaneously when the maximum allowable stress was reached, resulting in complete and immediate failure of the structure. As stochasticity was introduced, the onset of failure occurred at a lower load as weak individual strips failed, but adjacent strips allowed for more deformation and hence increased the maximum displacement. This resulted in lower strength (maximum force) but increased elongation to failure, and hence higher toughness (area under force-deformation curve).

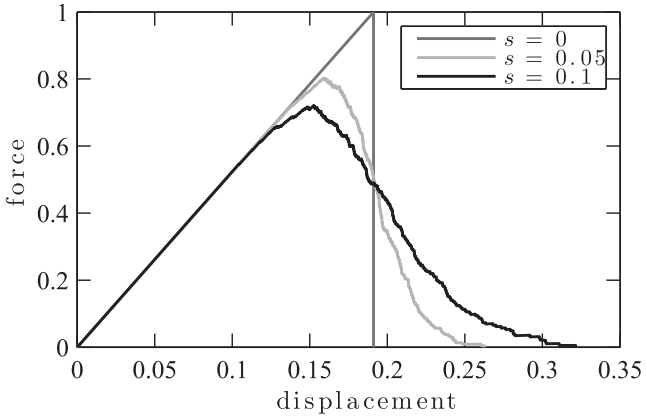

FIGURE 3 Results of three simulations with the same mean and different normalized standard deviation s in the distribution of the amplitude of 500 strips. For $s = 0$, the interface of every unit cell had the same height. Force increased linearly with displacement and was evenly distributed among all unit cells. When the maximum allowable stress was achieved, every strip failed simultaneously, resulting in an instantaneous drop in force. For $s = 0.05$, strips with the highest amplitude A failed first due to higher stress concentrations, resulting in a deviation from the linear relationship. Strips with lower-amplitude sustained loads to a larger displacement, allowing the model to reach a higher displacement before failure. When s was further increased to 0.1, the peak force was reached earlier and the maximum displacement was further increased.

We estimated the dependence of strength and toughness on the degree of interdigitation (A/λ) and stochasticity (standard deviation, s) by combining results from multiple force-displacement simulations. For each degree of interdigitation around the physiological range, a higher standard deviation in the distribution of A/λ yielded increasing loss in strength (Fig. 4). As given in the contour plot, this decrease in strength became more severe with increasing A/λ. However, a higher standard deviation in the distribution of A/λ also yielded increases in the toughness (measured as the total energy absorbed before failure). Furthermore, the rate of toughness increase was stronger for higher values of A/λ.

Stochasticity in the degree of interdigitation thus provided a trade-off between losses in strength and increases in toughness. Using the contour plots (Fig. 4), we compared strength loss and toughness at each combination of A/λ and s. Setting a criterion for the ratio of gain in toughness equaling that of the loss in strength, these plots could be combined to a single plot defining combinations of A/λ and s that lead to an enhanced interface. The A/λ versus standard deviation curve of Fig. 5 divides parameter space into two sections: strength loss outweighing the gain in toughness to the left of the curve, and toughness gain outweighing strength loss in the shaded region to the right of the curve. Physiological data for both young and old mice lie in the region for which toughness gain just outweigh strength loss (Fig. 5).

DISCUSSION

Results of the first-order model studied here demonstrate a trade-off between toughness and strength due to interdigitation at the attachment of tendon to bone: increasing the roughness and stochasticity of the bimaterial interface improves toughness at the cost of strength. If the parameters are carefully selected, it is possible that a gain in toughness outweighs the loss in strength. This appears to be the case for healthy mouse tendon-to-bone attachment.

In contrast to the natural attachment, contemporary surgical procedures introduce smooth and regular interfaces at the reattachment of tendon to bone, often by debridement and smoothing of the bony surface (39). This approach may not lead to an effectively repaired interface. The absence of interdigitation and stochasticity at the repair interface could contribute to the high failure rates after rotator cuff repair. Modeling results from this study suggest that this procedure can be optimized to enhance mechanical integrity of a surgical repair.

The results are unexpected when compared to analogous interdigitations between mineralized tissues. Examples of such interfaces are the suture lines of the skull, in which

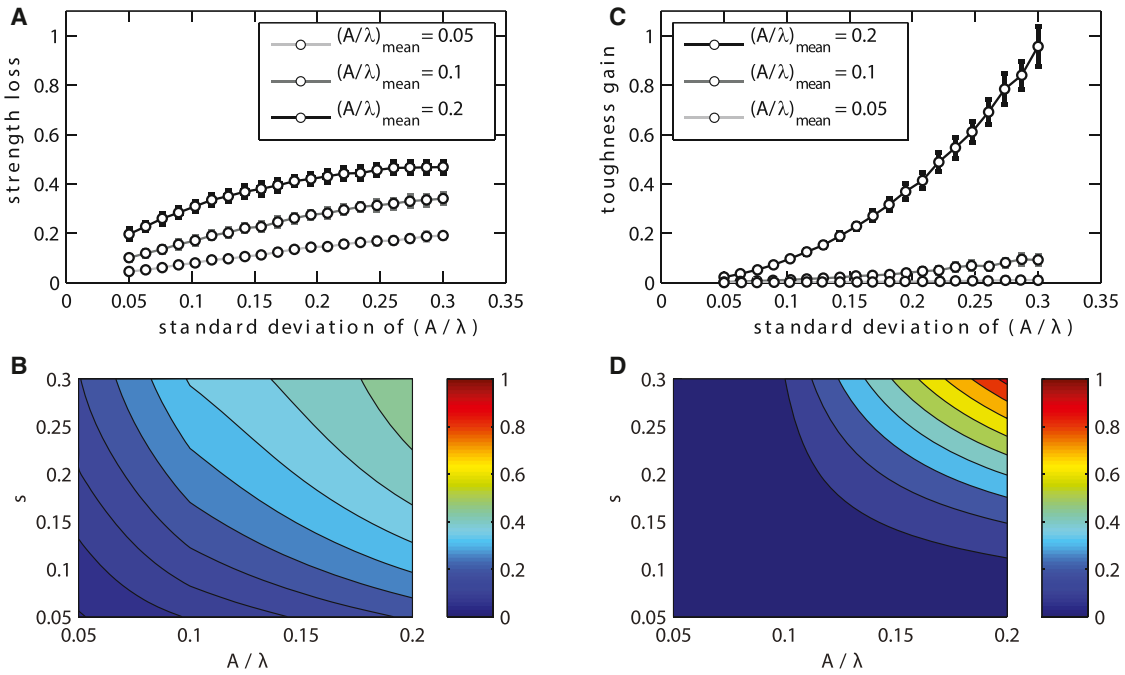

FIGURE 4 (*A*) As stochasticity of the degree of interdigitation (standard deviation *s* of *A*/λ) increased, the predicted strength (maximum stress) that the tendon-to-bone insertion could endure decreased. This effect was accentuated for higher mean values of *A*/λ. Error bars correspond to standard deviation from up to 20 replicate simulations. (*B*) Contours represent the mean strength loss expressed as a fraction of the strength of a tendon-to-bone attachment with a flat interface between tendon and bone. (*C*) As stochasticity of the degree of interdigitation (standard deviation *s* of *A*/λ) increased, the predicted toughness of the tendon-to-bone insertion increased. This effect was accentuated for higher mean values of *A*/λ. Error bars correspond to standard deviation from up to 20 replicate simulations. (*D*) Contours represent the mean toughness gain expected relative to the toughness of a tendon-to-bone attachment with a flat interface between tendon and bone. To see this figure in color, go online.

bones are separated by relatively compliant protein layers in gaps between interdigitations that appear to be more regular than those at the tendon-to-bone insertion site. Here, interfacial strength of cranial sutures is believed to be improved by the increase in surface area afforded by the interdigitation (28,30). However, this contrast is rectified by considering the differences between attachment of bone to bone versus attachment of tendon to bone. Based on shear lag analyses, the stress field within the compliant layer in a suture line is believed to be fairly uniform (compare to Genin and Liu (38)). Therefore, the entire volume of the compliant layer can be accessed before failure. However, the stress field at the interface of bone interdigitating into tendon presents local stress concentrations that we hypothesize might hasten local failures. Like the compliant layer within a suture line, we hypothesize that the presence of these stress concentrations on an interface with a distribution of roughness enables a greater volume of tissue to contribute to the overall toughness of the interface, thereby increasing the energy that must be absorbed before complete failure of the overall structure.

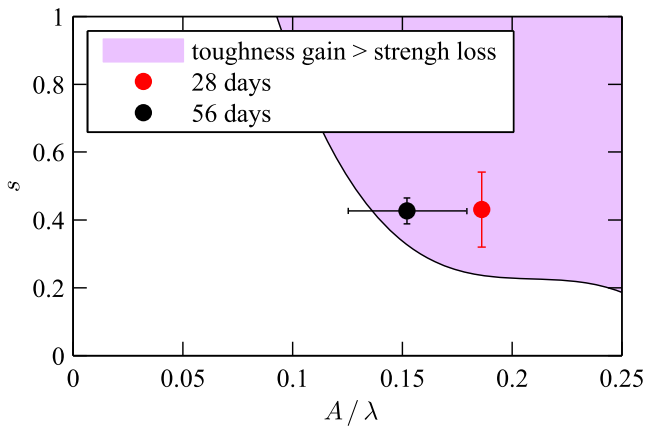

FIGURE 5 Using the contour plots (Fig. 4), the strength loss and toughness gain at each combination of *s* and *A*/λ were compared. (*Solid line*) Parameters that yield equivalent toughness gain and strength loss. (*Shaded region*) Combinations of *s* and *A*/λ for which the gain in toughness exceeds the loss of strength. The physiological values of *s* and *A*/λ (*symbols*) lie within this range. These values represent a sample size of >100 interdigitations in the six mice studied, which yields a margin of error <10% at the 95% confidence level. To see this figure in color, go online.

The results are consistent, however, when considered in the context of toughening at other hierarchical scales in bone. Bone and collagen both present highly structured hierarchical structures down to the nanoscale (40,41). At the nanoscale, heterogeneity is believed to enhance toughness (8,42), along with the stochastic nature of interactions between protein and mineral phases. At the mesoscale, stochastic mineral-to-mineral connections and other features that lead to heterogenous deformation may serve to enhance toughness (7,43,44). In this context, these results suggest

that the stochastic roughness at the attachment of tendon to bone might serve to extend these benefits of stochasticity to the gross tissue level.

The solutions that were implemented in this study focused on a level of analysis needed to elucidate the role of wavy interdigitations at the tendon-to-bone interface. A number of complexities of the tendon-to-bone attachment were not included in the model, most notably a gradient in mineral and in collagen fiber orientation (9,10). Although this gradient constitutes a central focus of many tissue engineering efforts (compare to Lipner et al. (45)), its origin is unclear. An ongoing uncertainty in the literature is whether the gradient in mineralization arises from interdigitating, fully mineralized features, or from a spatial gradient in mineral accumulation (9). These factors are particularly important for determining the local mechanical environment of cells in the interfacial region (e.g., Liu et al. (46)). We chose to focus this study on the simpler scenario of interdigitating tendon and bone, and note that a spatial gradient at the length scale of these interdigitations, should one be shown to exist, could negate the effects described in this article.

We note that the results presented in this study support an interesting hypothesis, but further numerical and experimental work is needed to determine whether this hypothesis can be falsified. Results are predicated upon linear models of the behavior and physiology of the natural tendon-to-bone interface. Real tissues certainly exhibit nonlinear and viscoelastic behavior, and the interface can be expected to exhibit toughness at deformation levels exceeding those corresponding to the onset of failure. However, we emphasize that the models capture the essence and qualitative aspects of the problem. The nonlinearity and orthotropy of tendon should serve to further amplify stress concentrations, with effects that should be analogous to increasing the degree of interdigitation. This study focused on mice, and we note that an allometric study of tendon-to-bone attachment is underway that spans many orders of magnitude in animal mass. Preliminary results indicate that the features described in this study for mice are similar in larger mammals, but whether these features serve similar roles in enhancing tendon-to-bone attachment across species is not yet known. An additional important question is the mechanical role of roughness exhibited at predominantly compressive interfaces like the osteochondral interface (47). These factors are important areas for future research.

CONCLUSIONS

The roughness that is observed at the tendon-to-bone interface appears to amplify stress concentrations relative to those that would occur at a smooth interface. On the other hand, stochasticity of the distribution of roughness may diminish the consequences of elevated interfacial stresses along the interface by increasing toughness. Furthermore, a rough and stochastic interface may serve as a potential toughening mechanism that has direct implications for the design of tendon-to-bone reattachment surgeries. More broadly, results point to the benefit of stochasticity in distributing stresses at an interface, and thereby accessing the toughness of a greater fraction of tissue.

SUPPORTING MATERIAL

Supporting Materials and Methods, ten equations, and eight figures are available at http://www.biophysj.org/biophysj/supplemental/S0006-3495(14)01135-7.

The authors are grateful to Weiqian Liu for assistance with the figures in this article.

This work was supported in part by the National Science Foundation (CAREER grant No. 844607), the National Institutes of Health (grant No. R01 AR055580), and a joint National Science Foundation-National Institutes of Health multiscale modeling grant (No. U01EB016422).

REFERENCES

1. Liu, Y., V. Birman, …, G. M. Genin. 2011. Mechanisms of bimaterial attachment at the interface of tendon to bone. *J. Eng. Mater. Technol.* 133:011006.
2. Thomopoulos, S., G. R. Williams, …, L. J. Soslowsky. 2003. Variation of biomechanical, structural, and compositional properties along the tendon to bone insertion site. *J. Orthop. Res.* 21:413–419.
3. Harryman, II, D. T., L. A. Mack, …, F. A. Matsen, III. 1991. Repairs of the rotator cuff (correlation of functional results with integrity of the cuff). *J. Bone Joint Surg. Am.* 73:982–989.
4. Monaco, E., L. Labianca, …, A. Ferretti. 2010. Biomechanical evaluation of different anterior cruciate ligament fixation techniques for hamstring graft. *J. Orthop. Sci.* 15:125–131.
5. Thomopoulos, S., G. Hattersley, …, L. J. Soslowsky. 2002. The localized expression of extracellular matrix components in healing tendon insertion sites: an in situ hybridization study. *J. Orthop. Res.* 20:454–463.
6. Galatz, L. M., C. M. Ball, …, K. Yamaguchi. 2004. The outcome and repair integrity of completely arthroscopically repaired large and massive rotator cuff tears. *J. Bone Joint Surg. Am.* 86-A:219–224.
7. Hang, F., H. S. Gupta, and A. H. Barber. 2014. Nanointerfacial strength between non-collagenous protein and collagen fibrils in antler bone. *J. R. Soc. Interface.* 11:20130993.
8. Buehler, M. J. 2007. Molecular nanomechanics of nascent bone: fibrillar toughening by mineralization. *Nanotechnology.* 18:295102.
9. Thomopoulos, S., J. P. Marquez, …, G. M. Genin. 2006. Collagen fiber orientation at the tendon to bone insertion and its influence on stress concentrations. *J. Biomech.* 39:1842–1851.
10. Genin, G. M., A. Kent, …, S. Thomopoulos. 2009. Functional grading of mineral and collagen in the attachment of tendon to bone. *Biophys. J.* 97:976–985.
11. Liu, Y. X., S. Thomopoulos, …, G. M. Genin. 2011. Bi-material attachment through a compliant interfacial system at the tendon-to-bone insertion site. *Mech. Mater.* 44: 01/2012.
12. Liu, Y., S. Thomopoulos, …, G. M. Genin. 2014. Modeling the mechanics of partially mineralized collagen fibrils, fibers and tissue. *J. R. Soc. Interface.* 11:20130835.
13. Ashby, M. F., and D. R. H. Jones. 2012. Engineering Materials 2: An Introduction to Microstructures and Processing. Butterworth-Heinemann, Oxford, UK.
14. McNulty, J. C., F. W. Zok, …, A. G. Evans. 1999. Notch-sensitivity of fiber-reinforced ceramic-matrix composites: effects of inelastic straining and volume-dependent strength. *J. Am. Ceram. Soc.* 82:1217–1228.

15. Rajan, V. P., and F. W. Zok. 2014. Stress distributions in bluntly-notched ceramic composite laminates. *Compos. A Appl. Sci. Manuf.* 60:15–23.

16. Genin, G. M., and J. W. Hutchinson. 1997. Composite laminates in plane stress: constitutive modeling and stress redistribution due to matrix cracking. *J. Am. Ceram. Soc.* 80:1245–1255.

17. Genin, G. M., and J. W. Hutchinson. 1999. Failures at attachment holes in brittle matrix laminates. *J. Compos. Mat.* 33:1600–1619.

18. Budiansky, B., J. W. Hutchinson, and A. G. Evans. 1986. Matrix fracture in fiber-reinforced ceramics. *J. Mech. Phys. Solids.* 34:167–189.

19. Coleman, B. D. 1958. On the strength of classical fibers and fiber bundles. *J. Mech. Phys. Solids.* 7:60–70.

20. Curtin, W. A. 1998. Stochastic damage evolution and failure in fiber-reinforced composites. *Adv. Appl. Mech.* 36:163–253.

21. Curtin, W. A. 1991. Theory of mechanical properties of ceramic-matrix composites. *J. Am. Ceram. Soc.* 74:2837–2845.

22. Ji, B., and H. Gao. 2004. Mechanical properties of nanostructure of biological materials. *J. Mech. Phys. Solids.* 52:1963–1990.

23. Wilbrink, D. V., M. Utz, …, M. R. Begley. 2010. Scaling of strength and ductility in bioinspired brick and mortar composites. *Appl. Phys. Lett.* 97:193701.

24. Song, J., S. Reichert, …, C. Ortiz. 2010. Quantitative microstructural studies of the armor of the marine threespine stickleback (*Gasterosteus aculeatus*). *J. Struct. Biol.* 171:318–331.

25. Garcia, A. P., N. Pugno, and M. J. Buehler. 2011. Superductile, wavy silica nanostructures inspired by diatom algae. *Adv. Eng. Mater.* 13:B405–B414.

26. Margulies, S. S., and K. L. Thibault. 2000. Infant skull and suture properties: measurements and implications for mechanisms of pediatric brain injury. *J. Biomech. Eng.* 122:364–371.

27. Skrzat, J., D. Holiat, and J. Walocha. 2003. A morphometrical study of the human palatine sutures. *Folia Morphol. (Warsz).* 62:123–127.

28. Li, Y., C. Ortiz, and M. C. Boyce. 2011. Stiffness and strength of suture joints in nature. *Phys. Rev. E Stat. Nonlin. Soft Matter Phys.* 84:062904.

29. Begley, M. R., N. R. Phillips, …, M. Utz. 2012. Micromechanical models to guide the development of synthetic 'brick and mortar' composites. *J. Mech. Phys. Solids.* 60:1545–1560.

30. Li, Y., C. Ortiz, and C. M. Boyce. 2013. A generalized mechanical model for suture interfaces of arbitrary geometry. *J. Mech. Phys. Solids.* 61:1144–1167.

31. Schneider, C. A., W. S. Rasband, and K. W. Eliceiri. 2012. NIH IMAGE to IMAGEJ: 25 years of image analysis. *Nat. Methods.* 9:671–675.

32. Gurton, E. M., E. Fried, and L. Anand. 2010. The Mechanics and Thermodynamics of Continua. Cambridge University Press, New York.

33. Gao, H. 1991. A boundary perturbation analysis for elastic inclusions and interfaces. *Int. J. Solids Struct.* 28:703–725.

34. Oyen, M. L., V. L. Ferguson, …, A. Boyde. 2008. Composite bounds on the elastic modulus of bone. *J. Biomech.* 41:2585–2588.

35. Katz, J. L. 1971. Hard tissue as a composite material. I. Bounds on the elastic behavior. *J. Biomech.* 4:455–473.

36. Hellmich, C., and F.-J. Ulm. 2002. Micromechanical model for ultrastructural stiffness of mineralized tissues. *J. Eng. Mech.* 128:898–908.

37. Genin, G. M., and V. Birman. 2009. Micromechanics and structural response of functionally graded, particulate-matrix, fiber-reinforced composites. *Int. J. Solids Struct.* 46:2136–2150.

38. Genin, G. M., and Y. Liu. 2013. Models for the mechanics of joining dissimilar materials. *In* Structural Interfaces and Attachments in Biology. Springer, New York, pp. 43–66.

39. Iyengar, J. J., S. P. Samagh, …, B. T. Feeley. 2014. Current trends in rotator cuff repair: surgical technique, setting, and cost. *Arthroscopy.* 30:284–288.

40. Schwartz, A. G., J. D. Pasteris, …, S. Thomopoulos. 2012. Mineral distributions at the developing tendon enthesis. *PLoS ONE.* 7:e48630.

41. Alexander, B., T. L. Daulton, …, S. Thomopoulos. 2012. The nanometer-scale physiology of bone: steric modeling and scanning transmission electron microscopy of collagen-mineral structure. *J. R. Soc. Interface.* 9:1774–1786.

42. Tai, K., M. Dao, …, C. Ortiz. 2007. Nanoscale heterogeneity promotes energy dissipation in bone. *Nat. Mater.* 6:454–462.

43. Fantner, G. E., T. Hassenkam, …, P. K. Hansma. 2005. Sacrificial bonds and hidden length dissipate energy as mineralized fibrils separate during bone fracture. *Nat. Mater.* 4:612–616.

44. Hang, F., and A. H. Barber. 2011. Nano-mechanical properties of individual mineralized collagen fibrils from bone tissue. *J. R. Soc. Interface.* 8:500–505.

45. Lipner, J., W. Liu, …, S. Thomopoulos. 2014. The mechanics of PLGA nanofiber scaffolds with biomimetic gradients in mineral for tendon-to-bone repair. *J. Mech. Behav. Biomed. Mater.* 40C:59–68.

46. Liu, Y., A. G. Schwarz, …, G. M. Genin. 2013. Stress amplification during development of the tendon-to-bone attachment. *Biomech. Model. Mechanobiol.* 13:973–983.

47. Campbell, S. E., V. L. Ferguson, and D. C. Hurley. 2012. Nanomechanical mapping of the osteochondral interface with contact resonance force microscopy and nanoindentation. *Acta Biomater.* 8:4389–4396.